Cone-beam reconstruction by backprojection and filtering

Andrei V. Bronnikov

KEMA, Utrechtseweg 310, P.O. Box 9035, 6800 ET Arnhem, The Netherlands

A new analytical method for tomographic image reconstruction from cone-beam projections acquired on the source orbits lying on a cylinder is presented. By application of a weighted cone-beam backprojection, the reconstruction problem is reduced to an image-restoration problem characterized by a shift-variant point-spread function that is given analytically. Assuming that the source is relatively far from the imaged object, a formula for an approximate shift-invariant inverse filter is derived; the filter is presented in the Fourier domain. Results of numerical experiments with circular and helical orbits are considered. © 2000 Optical Society of America [S0740-3232(00)01111-X]

OCIS codes: 110.6960, 100.3010.

1. INTRODUCTION

Three-dimensional (3D) image reconstruction from cone-beam projections is one of the latest generalizations of computed tomography (CT). In medical CT, cone-beam projections can be acquired by translating the patient through a gantry comprising the x-ray source and a two-dimensional (2D) detector, which captures a cone of x-rays penetrating through the whole 3D field of view of the system. This geometry provides certain advantages over conventional collimator-based CT, increasing the photon flux, shortening acquisition time, and making possible the geometrical magnification of projections. The latter is also useful in imaging with radioisotopes, known as single-photon-emission computed tomography (SPECT), where the application of a cone-beam collimator increases the total number of measured photons, improving both the spatial resolution and the quantitative characteristics of images.[1,2] Compared with slice-by-slice scanning, cone-beam geometry facilitates data acquisition but, at the same time, creates certain difficulties for solution of the corresponding image-reconstruction problem. Mathematically speaking, the cone-beam reconstruction problem is to find the object function f from the equation

$$g(\mathbf{s}, \mathbf{u}) = \int_0^\infty f(\mathbf{s} + t\mathbf{u}) \mathrm{d}t \tag{1}$$

that describes integration over the half-line with starting point $\mathbf{s}$ and direction $\mathbf{u} \in S^2$, where S^2 stands for the unit sphere in $\mathcal{R}^3$. Figure 1 depicts the geometry of imaging where vector $\mathbf{s} \in \mathcal{R}^3$ represents a single source location on the orbit and $f(\mathbf{r})$, $\mathbf{r} = (x, y, z) \in \mathcal{R}^3$ can be interpreted as the 3D image. Function f vanishes outside the unit ball:

$$f(\mathbf{r}) = 0 \qquad \text{for} \quad |\mathbf{r}| > 1. \tag{2}$$

One of the ways of inverting integral equation (1) is to resort to the 3D Radon transform, which reads as

$$\check{f}(\mathbf{n}, s) = \int_{\mathcal{R}^3} f(\mathbf{r}) \delta(s - \mathbf{r} \cdot \mathbf{n}) \mathrm{d}\mathbf{r}, \tag{3}$$

where the centered dot denotes the scalar product.[3] The 3D Radon transform describes the integration of $f(\mathbf{r})$ over a plane that is perpendicular to the vector $\mathbf{n} \in S^2$ and lies a distance s from the origin. The inversion of Eq. (3) has been known from the beginning of the century, when J. Radon and H. A. Lorentz independently found that $f(\mathbf{r}) = -1/(8\pi^2)\nabla^2 \int_{S^2} \check{f}(\mathbf{n}, \mathbf{r} \cdot \mathbf{n}) \mathrm{d}\mathbf{n}$, where ∇^2 is the Laplacian acting on $\mathbf{r}$. To make use of this formula, which is often referred to as the inverse Radon transform, one needs to establish a connection between the Radon transform and Eq. (1). This connection is given by the following

Theorem:

If γ is a homogeneous distribution of degree -2, i.e., $\gamma(ts) = t^{-2}\gamma(s)$, then

$$\gamma * \check{f}(\mathbf{n}, \mathbf{s} \cdot \mathbf{n}) = \int_{S^2} \gamma(\mathbf{u} \cdot \mathbf{n}) g(\mathbf{s}, \mathbf{u}) \mathrm{d}\mathbf{u}, \tag{4}$$

where $*$ denotes the convolution over the second variable of the Radon transform.[4–6] Let us observe that in combination with the inverse Radon transform, the theorem gives us a general method of finding function f from its cone-beam projections. Several choices of function γ can be considered, leading to different reconstruction algorithms. In particular, the choice $\gamma(s) = \delta'(s)$ gives us the Grangeat reconstruction formula,[7] and $\gamma(s) = \int_{-\infty}^{+\infty} |\sigma| \exp(-is\sigma) \mathrm{d}\sigma$ defines algorithms suggested by Feldkamp *et al.*[8] and Smith.[9] Bronnikov and Duifhuis examined the latter approach in combination with wavelet-based filtering using $\gamma_{2^j}(s) = \int_{-\infty}^{+\infty} W(2^j\sigma)|\sigma| \exp(-is\sigma) \mathrm{d}\sigma$, where $W(2^j\sigma)$ is the Fourier transform of the wavelet at the jth scale.[10]

For a complete set of cone-beam projections to be obtained certain geometrical conditions have to be met. As early as 1961, A. A. Kirillov formulated such conditions in his pioneering work on cone-beam reconstruction of a
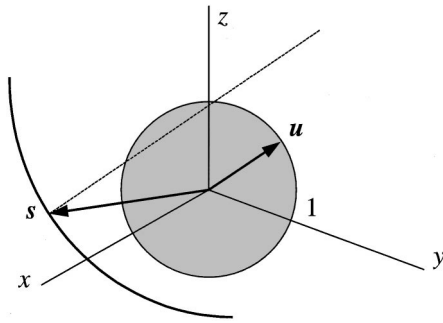
Fig. 1. Geometry of cone-beam scanning. The support of function $f(\mathbf{r})$ is shown as a gray ball. The position of the source on the path about the object is given by vector $\mathbf{s}$. The line integral is taken along the dashed line that is parallel to unit vector $\mathbf{u}$. A cone-beam projection of the object is collected by rotating vector $\mathbf{u}$.

complex-valued n-dimensional function.[11] Later, similar conditions were applied in image reconstruction, where they are often referred to as "Kirillov–Tuy's completeness conditions." [12,13] Another form of completeness condition for a discrete problem was proposed by Barrett and Gifford.[14] The Kirillov–Tuy conditions can be expressed as follows: "The cone-beam data are complete and the corresponding inverse problem has an exact solution if every plane that is orthogonal to vector $\mathbf{n} \in S^2$ and lies on the distance $|s| \leq 1$ from the origin intersects the source path at least in one point." To explain the nature of these conditions, we observe that the scalar product $\mathbf{s} \cdot \mathbf{n} = s$ on the left-hand side of Eq. (4) describes such a plane. Thus, to recover the Radon transform over all planes intersecting the unit ball, we require that every equation $\mathbf{s} \cdot \mathbf{n} = s$ with $|s| \leq 1$ has at least one solution with respect to the source locus $\mathbf{s}$. For instance, a unit sphere that coincides with the support of the image presents a complete geometry: All planes that intersect the unit ball will intersect the source path. On the other hand, a circular orbit gives us an example of incomplete geometry: There are planes (which are parallel to the plane of the circle) intersecting the object but not the source orbit. In this case, an accurate inversion is not possible. However, satisfactory results can be obtained if the source is relatively far from the reconstructed object.[8,10,15,16] Kirillov–Tuy orbits can be implemented by a nonplanar motion of the source. Several examples of such orbits are considered in the literature.[9,13,17–22] In this paper we shall consider the parametric representation $\mathbf{s} = \mathbf{s}(\theta)$, $\theta \in \Theta$ and implement the scanning on a cylinder, which yields

$$\mathbf{s}(\theta) = [R \cos \theta, \, R \sin \theta, \, \tau(\theta)]^T, \qquad \theta \in \Theta, \qquad (5)$$

where R is the radius of the cylinder and $\tau(\theta)$ is the axial position of the source. The set Θ can be defined in a way that allows us to implement various scanning configurations; we shall consider examples of circular and helical scanning in Section 5.

Accurate reconstruction algorithms based on Eq. (4) require complex and long computations. As was shown by Defrise and Clack,[22] the main difficulty here is the nonstationary nature of the problem. At the same time, as has been shown by several authors, the use of the fast

Fourier transform for computing the Radon transform can accelerate the reconstruction.[22–26] However, no closed-form algorithm similar to conventional filtered backprojection can be found here without resorting to an approximation. The latter can be achieved, for instance, by using a rebinning algorithm, as was shown by Noo et al.[27] Since Feldkamp et al.[8] proposed their approximate filtered backprojection algorithm for the single circle, several similar methods have been suggested for different orbits[20,21] however, to my knowledge, very few backprojection-and-filtering algorithms, which first perform backprojection and then filtering, have been studied in the present context, although they have been actively studied for parallel-beam and fan-beam reconstruction.[28,29] So far, mostly a spherical configuration of a cone-beam detector has been applied for derivation of backprojection-and-filtering algorithms.[30,31] For instance, Peyrin[30] considered a generalization of the rho-filtered backprojection for both 4π parallel and divergent geometries. A weighted backprojection was performed, and then a 3D filtering was carried out in the Fourier domain by applying a filter with modulation transfer function (MTF) $|\mathbf{k}|$, where $\mathbf{k} = (k_x, k_y, k_z)$ is a vector of spatial frequencies. Cho et al.[31] generalized this result for the case of truncated spherical geometry. Their algorithm was also based on the use of a weighted backprojection, after which they applied the Colsher filter, which is nothing but $|\mathbf{k}|$ weighted by a factor dependent on the acceptance angle. Although satisfactory results were obtained in a number of experiments with mathematical phantoms, both geometries—complete and truncated spheres—remain impractical in SPECT and redundant in CT. Another approach was presented by Peyrin et al.,[32] where the authors found an analytical description for the point-spread function (PSF) of a cone-beam system with source orbits such as a circle and two orthogonal circles. In this method, a shift-invariant approximation of a shift-variant PSF was used for cone-beam reconstruction under the assumption that the cone-beam geometry can be replaced by a parallel-beam geometry.[32] In contrast to the result of Peyrin et al.,[32] here a general description is provided of the PSF for any source orbits that lie on a cylinder wrapping the object. Furthermore, a weighting factor in backprojection is introduced that allows us to simplify the description of the PSF and consequently to obtain a unique and simple expression for the MTF of the approximate shift-invariant reconstruction filter for different data-acquisition geometries. Our reconstruction algorithm can be described by the following diagram:

$$g(\mathbf{s},\mathbf{u}) \xrightarrow{\text{backprojection}} f_s(\mathbf{r}) \xrightarrow{\text{deblurring}} f(\mathbf{r}).$$

In the deblurring step of the algorithm an imaging equation is introduced, allowing us to describe a reconstruction problem as an image-restoration problem with a shift-variant PSF. After applying the approximation, we are able to formulate the problem in the form of a convolution equation that can be solved efficiently by using the fast Fourier transform. A formula for the reconstruction filter is given, and the method is numerically evaluated for the circular and helical source orbits.

2. IMAGING EQUATION

Using representation (5), we can rewrite the basic equation [Eq. (1)] in the form of the cone-beam transform

$$g(\mathbf{s}(\theta), \mathbf{u}) = \int_0^\infty f(\mathbf{s}(\theta) + t\mathbf{u})\mathrm{d}t, \qquad \theta \in \Theta, \qquad \mathbf{u} \in S^2$$

$$(6)$$

on orbit $\mathbf{s}(\theta)$. Consider the x-ray transform

$$\hat{f}(\mathbf{s}(\theta), \mathbf{u}) = \int_{-\infty}^{+\infty} f(\mathbf{s}(\theta) + t\mathbf{u})\mathrm{d}t, \qquad (7)$$

where the integration is carried out over the whole line passing through the point $\mathbf{s}(\theta)$. Comparing equations (6) and (7), we may write

$$\hat{f}(\mathbf{s}(\theta), \mathbf{u}) = g(\mathbf{s}(\theta), \mathbf{u}) + g(\mathbf{s}(\theta), -\mathbf{u}). \qquad (8)$$

To derive our image-reconstruction algorithm, we use notation of the delta function, which allows us to rewrite Eq. (7) in the form

$$\hat{f}(\mathbf{s}(\theta), \mathbf{u}) = \int_{-\infty}^{+\infty} \int_{\mathcal{R}^3} f(\mathbf{r})\delta(\mathbf{r} - \mathbf{s}(\theta) - t\mathbf{u})\mathrm{d}r\mathrm{d}t$$

$$= \int_{\mathcal{R}^3} f(\mathbf{r}) \int_{-\infty}^{+\infty} \delta(\mathbf{r} - \mathbf{s}(\theta) - t\mathbf{u})\mathrm{d}t\mathrm{d}r. \qquad (9)$$

Let us define a backprojection image $f_s(\mathbf{r})$, which can be found by averaging values of the x-ray transform at the point $\mathbf{r}$. The index s in $f_s(\mathbf{r})$ indicates the dependence of the backprojection on a particular source path. Function $f_s(\mathbf{r})$ can be defined as

$$f_s(\mathbf{r}) = \int_\Theta \frac{1}{|\mathbf{r} - s(\theta)|} \hat{f}\left(\mathbf{s}(\theta), \frac{\mathbf{r} - \mathbf{s}(\theta)}{|\mathbf{r} - \mathbf{s}(\theta)|}\right)\mathrm{d}\theta. \qquad (10)$$

It should be pointed out that the cone-beam backprojection used in a filtered backprojection algorithm requires a weighting coefficient $|\mathbf{r} - \mathbf{s}(\theta)|^{-2}$ (Ref. 22). Nevertheless, we are at liberty to define a backprojection operator, applying weighting factor that simplifies the formula for the reconstruction filter. The relation of $f_s(\mathbf{r})$ to the cone-beam data g can be found by inserting Eq. (8) into Eq. (10), which yields

$$f_s(\mathbf{r}) = \int_\Theta \frac{1}{|\mathbf{r} - \mathbf{s}(\theta)|}\left[g\left(\mathbf{s}(\theta), \frac{\mathbf{r} - \mathbf{s}(\theta)}{|\mathbf{r} - \mathbf{s}(\theta)|}\right)\right.$$

$$+ \left. g\left(\mathbf{s}(\theta), \frac{\mathbf{s}(\theta) - \mathbf{r}}{|\mathbf{r} - \mathbf{s}(\theta)|}\right)\right]\mathrm{d}\theta$$

$$= \int_\Theta \frac{1}{|\mathbf{r} - \mathbf{s}(\theta)|} g\left(\mathbf{s}(\theta), \frac{\mathbf{r} - \mathbf{s}(\theta)}{|\mathbf{r} - \mathbf{s}(\theta)|}\right)\mathrm{d}\theta,$$

where we have assumed that the orbit lies on a surface that completely covers the object and therefore

$$g\left(\mathbf{s}(\theta), \frac{\mathbf{s}(\theta) - \mathbf{r}}{|\mathbf{r} - \mathbf{s}(\theta)|}\right) = 0.$$

Inserting Eq. (9) into Eq. (10), we find

$$f_s(\mathbf{r}) = \int_\Theta \frac{1}{|\mathbf{r} - \mathbf{s}(\theta)|} \int_{\mathcal{R}^3} f(\mathbf{r}') \int_{-\infty}^{+\infty} \delta\left(\mathbf{r}' - \mathbf{s}(\theta)\right.$$

$$\left. - t\frac{\mathbf{r} - \mathbf{s}(\theta)}{|\mathbf{r} - \mathbf{s}(\theta)|}\right)\mathrm{d}t\mathrm{d}\mathbf{r}'\mathrm{d}\theta$$

$$= \int_{\mathcal{R}^3} f(\mathbf{r}') \int_\Theta \int_{-\infty}^{+\infty} \delta\left(\mathbf{r}' - \mathbf{s}(\theta)\right.$$

$$\left. - t'(\mathbf{r} - \mathbf{s}(\theta))\right)\mathrm{d}t'\mathrm{d}\theta\mathrm{d}\mathbf{r}',$$

where we have used the change of variable $t' = t/|\mathbf{r} - \mathbf{s}(\theta)|$. Note that the weighting factor in backprojection has been eliminated by the change of variable. The integral over t' can be rewritten as

$$\int_{-\infty}^{+\infty} \delta(\mathbf{r}' - \mathbf{s}(\theta) - t(\mathbf{r} - \mathbf{s}(\theta)))\mathrm{d}t$$

$$= \int_{-\infty}^{+\infty} \delta(\mathbf{r}' - \mathbf{r} + \mathbf{r} - \mathbf{s}(\theta) - t(\mathbf{r} - \mathbf{s}(\theta)))\mathrm{d}t$$

$$= \int_{-\infty}^{+\infty} \delta(\mathbf{r}' - \mathbf{r} - (t - 1)(\mathbf{r} - s(\theta)))\mathrm{d}t$$

$$= \int_{-\infty}^{+\infty} \delta(\mathbf{r} - \mathbf{r}' + t'(\mathbf{r} - \mathbf{s}(\theta)))\mathrm{d}t',$$

which gives us an integral equation

$$\int_{\mathcal{R}^3} f(\mathbf{r}')h_s(\mathbf{r}, \mathbf{r} - \mathbf{r}')\mathrm{d}\mathbf{r}' = f_s(\mathbf{r}), \qquad (11)$$

with the kernel

$$h_s(\mathbf{r}, \mathbf{r}_0) = \int_\Theta \int_{-\infty}^{+\infty} \delta(\mathbf{r}_0 + t(\mathbf{r} - \mathbf{s}(\theta)))\mathrm{d}t\mathrm{d}\theta. \qquad (12)$$

The function $h_s(\mathbf{r}, \mathbf{r}_0)$ can be interpreted as a shift-variant PSF of a cone-beam imaging system. If h_s were not a function of $\mathbf{r}$, then Eq. (11) would be a convolution, which would greatly simplify matters. However, this is not the case, and we need to apply certain conditions under which a suitable approximation to a convolution equation can be found, as will be done in Section 4.

3. POINT-SPREAD FUNCTION

Let us rewrite Eq. (12) using Eq. (5), which yields

$$h_s(\mathbf{r}, \mathbf{r}_0) = \int_\Theta \int_{-\infty}^{+\infty} \delta(x_0 + t(x - R\cos\theta))$$

$$\times \ \delta(y_0 + t(y - R\sin\theta))$$

$$\times \ \delta(z_0 + t(z - \tau(\theta)))\mathrm{d}t\mathrm{d}\theta. \qquad (13)$$

The inner integral in Eq. (13) can be evaluated as

$$\int_{-\infty}^{+\infty} \delta(x_0 + t(x - R\cos\theta))\delta(y_0 + t(y - R\sin\theta))$$

$$\times \ \delta(z_0 + t(z - \tau(\theta)))dt$$

$$= \frac{1}{|y - R\sin\theta|}\int_{-\infty}^{+\infty}\delta(x_0 + t(x - R\cos\theta))$$

$$\times \ \delta(z_0 + t(z - \tau(\theta)))\delta\!\left(t + \frac{y_0}{y - R\sin\theta}\right)dt$$

$$= \delta((y - R\sin\theta)x_0 - (x - R\cos\theta)y_0)$$

$$\times \ \delta\!\left(z_0 - \frac{z - \tau(\theta)}{y - R\sin\theta}y_0\right).$$

Now the integral over θ can be evaluated. To this end, we rewrite Eq. (13) as

$$h_s(\mathbf{r}, \mathbf{r}_0) = \frac{1}{(x_0^2 + y_0^2)^{1/2}}\int_\Theta \delta\!\left(z_0 - \frac{z - \tau(\theta)}{y - R\sin\theta}y_0\right)$$

$$\times \ \delta\!\left(\frac{(y - R\sin\theta)x_0}{(x_0^2 + y_0^2)^{1/2}} - \frac{(x - R\cos\theta)y_0}{(x_0^2 + y_0^2)^{1/2}}\right)d\theta,$$

where we have multiplied and divided the argument of the second delta function by $(x_0^2 + y_0^2)^{1/2}$. Using $\phi = \arctan(y_0/x_0)$, so that $\cos\phi = x_0/(x_0^2 + y_0^2)^{1/2}$ and $\sin\phi = y_0/(x_0^2 + y_0^2)^{1/2}$, we can evaluate the integral as

$$\int_\Theta \delta\!\left(z_0 - \frac{z - \tau(\theta)}{y - R\sin\theta}y_0\right)\delta((y - R\sin\theta)$$

$$\times \ \cos\phi - (x - R\cos\theta)\sin\phi)d\theta$$

$$= \frac{1}{R}\int_\Theta \delta\!\left(z_0 - \frac{z - \tau(\theta)}{y - R\sin\theta}y_0\right)\delta(\sin(\phi - \theta)$$

$$+ \ (y\cos\phi - x\sin\phi)/R)d\theta$$

$$= \frac{1}{R}\int_\Theta \delta\!\left(z_0 - \frac{z - \tau(\theta)}{y - R\sin\theta}y_0\right)$$

$$\times \ \sum_{n=1}^{2}\frac{\delta(\theta - \theta_m)}{|\cos(\phi - \theta_m)|}d\theta$$

$$= \frac{1}{[R^2 - (xy_0 - yx_0)^2/(x_0^2 + y_0^2)]^{1/2}}$$

$$\times \ \sum_{n=1}^{2}\delta\!\left(z_0 - \frac{z - \tau(\theta_m)}{y - R\sin\theta_m}y_0\right).$$

Here we have used the relation $\delta(a(b)) = \Sigma_{m=1}^{M}\delta(b - b_m)/|da/db(b_m)|$, where b_m are roots of the equation $a(b) = 0$. In this way, $0 < \theta_m \leqslant 2\pi$ must be the roots of the equation

$$\sin(\phi - \theta) + (y\cos\phi - x\sin\phi)/R = 0;$$

therefore

$$\theta_m = \arcsin\!\left[\frac{y_0}{(x_0^2 + y_0^2)^{1/2}}\right] - \arcsin\!\left[\frac{xy_0 - yx_0}{R(x_0^2 + y_0^2)^{1/2}}\right]$$

$$+ \ (m - 1)\pi, \ m = 1, 2 \qquad (14)$$

and

$$|\cos(\phi - \theta_m)| = \left|\cos\!\left\{\arcsin\!\left[\frac{xy_0 - yx_0}{R(x_0^2 + y_0^2)^{1/2}}\right]\right\}\right|$$

$$= \left[1 - \frac{1}{R^2}\frac{(xy_0 - yx_0)^2}{x_0^2 + y_0^2}\right]^{1/2}.$$

Thus the final expression for the PSF is

$$h_s(\mathbf{r}, \mathbf{r}_0) = \frac{1}{[R^2(x_0^2 + y_0^2) - (xy_0 - yx_0)^2]^{1/2}}$$

$$\times \ \sum_{m=1}^{2}\delta\!\left(z_0 - \frac{z - \tau(\theta_m)}{y - R\sin\theta_m}y_0\right). \qquad (15)$$

The expression of the PSF given by Eq. (15) has a clear structure: The sum of the delta functions is responsible for representation of the blurring in the direction of the z axis, whereas the multiplicative factor before the sum describes the blurring in the transaxial planes. Such simplicity of the PSF structure is due to the specially chosen weighting factor in backprojection and because of the formulation of the reconstruction problem for a cylindrical support of the source orbit. As seen from the paper by Peyrin et al.,[32] the use of a general form of backprojection with a spherical support of the source orbit leads to a more cumbersome expression for the PSF. Unlike the result by Peyrin et al.,[32] which was derived only for circular orbits, Eq. (15) describes the PSF of a cone-beam system for arbitrary orbits given by Eq. (5).

4. SHIFT-INVARIANT APPROXIMATION

In this section we consider a shift-invariant approximation to the function $h_s(\mathbf{r}, \mathbf{r}_0)$, which allows us to ignore the dependence on $\mathbf{r}$, reducing Eq. (11) to convolution. Let us assume that

$$R \gg 1, \qquad (16)$$

i.e., the radius of the cylindrical support of the source path is much larger than the radius of the spherical support of function f. Then Eq. (14) can be reduced to

$$\tilde{\theta}_m = \arcsin\!\left[\frac{y_0}{(x_0^2 + y_0^2)^{1/2}}\right] + (m - 1)\pi, \qquad (17)$$

which yields

$$\sin(\tilde{\theta}_m) = \frac{y_0}{(x_0^2 + y_0^2)^{1/2}}. \qquad (18)$$

Using $\tilde{\theta}_m$, we can rewrite the sum in Eq. (15) as

$$\sum_{m=1}^{2}\delta\!\left(z_0 - \frac{z - \tau(\tilde{\theta}_m)}{y - R\sin\tilde{\theta}_m}y_0\right)$$

$$\approx \sum_{m=1}^{2}\delta\!\left(z_0 + \frac{1}{R}(x_0^2 + y_0^2)[z - \tau(\tilde{\theta}_m)]\right)$$

$$\approx 2\delta(z_0). \qquad (19)$$

On the other hand,

$$[R^2(x_0{}^2 + y_0{}^2) - (xy_0 - yx_0)^2]^{1/2} \approx R(x_0{}^2 + y_0{}^2)^{1/2} \tag{20}$$

if inequality (16) holds. Thus, using approximations given by relations (19) and (20), we arrive at the desired function

$$\tilde{h}_s(\mathbf{r}_0) = \frac{2}{R} \frac{\delta(z_0)}{(x_0{}^2 + y_0{}^2)^{1/2}}, \tag{21}$$

which describes a shift-invariant approximation to the PSF. Using the function $\tilde{h}_s(\mathbf{r}_0)$ instead of the PSF $h_s(\mathbf{r}, \mathbf{r}_0)$ in Eq. (11), we can reduce the latter to the convolution. The presence of the delta function $\delta(z_0) = \delta(z - z')$ suggests that 3D filtering in Eq. (11) is reduced to 2D filtering of transaxial planes. Thus Eq. (11) can be approximated in the Fourier domain by the convolution equation

$$\tilde{H}_s(k_x, k_y)F(k_x, k_y, z) \approx F_s(k_x, k_y, z),$$

where $\tilde{H}_s(k_x, k_y)$ is the Fourier transform

$$\tilde{H}_s(k_x, k_y) = \frac{2}{R} \frac{2\pi}{(k_x{}^2 + k_y{}^2)^{1/2}} \tag{22}$$

of the approximate PSF and F and F_s are the Fourier transforms in the transaxial planes of the image f and the backprojection f_s, respectively.

The weighting factor in backprojection equation (10) also has to be changed in order to reflect the approximation made. It is easy to show that if inequality (16) holds, then

$$|\mathbf{r} - \mathbf{s}(\theta)| \approx \{R^2 + [z - \tau(\theta)]^2\}^{1/2}.$$

The factor $2/R$ can be taken out of expression (22), inverted, and inserted into the weighting factor in backprojection, which then becomes

$$\frac{R}{2\{R^2 + [z - \tau(\theta)]^2\}^{1/2}}.$$

5. ALGORITHM

The reconstruction algorithm can be described by the following two steps:

1. Weighted backprojection

$$\tilde{f}_s(\mathbf{r}) = \frac{R}{2} \int_\Theta \frac{1}{\{R^2 + [z - \tau(\theta)]^2\}^{1/2}} g\left(\frac{\mathbf{r} - \mathbf{s}(\theta)}{|\mathbf{r} - \mathbf{s}(\theta)|}, \theta\right) d\theta.$$

2. Filtering

(a) $\tilde{F}_s(k_x, k_y, z) = (2\pi)^{-1} \int_{-\infty}^{\infty} \int_{-\infty}^{\infty} \tilde{f}_s(\mathbf{r})$

$$\times \exp[-i(k_x x + k_y y)]dxdy;$$

(b) $\tilde{F}(k_x, k_y, z) = I_s(\sqrt{k_x{}^2 + k_y{}^2})A(\sqrt{k_x{}^2 + k_y{}^2})$

$$\times \tilde{F}_s(k_x, k_y, z);$$

(c) $\tilde{f}(r) = (2\pi)^{-1} \int_{-\infty}^{\infty} \int_{-\infty}^{\infty} \tilde{F}(k_x, k_y, z)$

$$\times \exp[i(k_x x + k_y y)]dk_x dk_y,$$

where

$$I_s(\rho) = \frac{\rho}{2\pi} \tag{23}$$

describes the inverse filter and $A(\rho)$ is the MTF of the apodization window. For instance, we can employ the von Hann window

$$A(\rho) = \begin{cases} 0.5 + 0.5\cos(\pi\rho/\Omega) & \text{for } \rho \le \Omega \\ 0 & \text{for } \rho > \Omega, \end{cases}$$

where Ω is the cutoff frequency.

Consider two particular implementations of our algorithm, which are based on the circular and helical data-acquisition orbits. A circular scan can be described by Eq. (5) with

$$\tau(\theta) = 0,$$

$$\Theta = \{\theta : 0 \le \theta < 2\pi\}.$$

This is an example of an incomplete geometry that, however, allows simple implementation. As an example of a nonplanar orbit, we will use a helix with n turns about the object. Let us assume that the backprojection is done with successive 2π segments of the helix. Such a geometry can be described by Eq. (5) with ($n > 1$)

$$\tau(\theta) = \left(1 + \frac{1}{n-1}\right)\left(\frac{\theta}{\pi n} - 1\right),$$

$$\Theta = \{\theta : \lambda(z) \le \theta < \lambda(z) + 2\pi\},$$

where

$$\lambda(z) = \pi n \left(\frac{z - 1/(n-1)}{1 + 1/(n-1)} + 1\right)$$

is chosen in such a way that we can center the 2π segment on a z slice. The multiplication factor $1 + 1/(n-1)$ in function τ serves to ensure completeness of all 2π segments for transaxial slices lying in the interval $-1 \le z < 1$.

6. EVALUATION

To evaluate the performance of the suggested algorithm, we have applied two numerical phantoms, as used by Kudo and Saito,[18] to study exact reconstruction methods based on Eq. (4). For geometrical parameters of the phantoms, we refer to the work by Kudo and Saito.[18] The first phantom consists of several balls with different densities simulating the bone structure, tissue, and tumors. The bone is represented by a value of 2.0, and the differences between the structures representing the tissue are relatively small: The normal tissue is represented by a value of 1.02, and anomalies are represented by densities of 1.04 and 1.00, which is consistent with the practical situation in medical CT. The object is centered on the origin, and its radius is equal to 0.9. Twelve
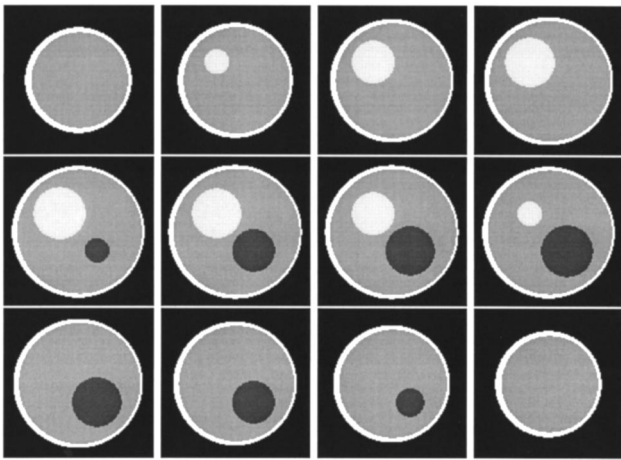
Fig. 2. Numerical phantom used in the simulation studies. The bone is represented by a value of 2.0, and the normal tissue is represented by a value of 1.02, with a maximum density of 1.04 and a minimum density of 1.00. The object is centered on the origin, and its radius is equal to 0.9. The x–y planes are shown for $z = 0.1k - 0.55$, $k = 0, 1, ..., 11$. Image values between 0.99 and 1.05 are displayed.
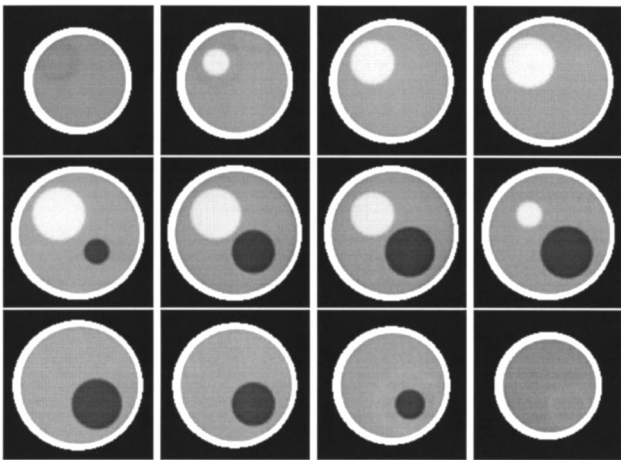
Fig. 3. Reconstructed images of the phantom. The reconstruction was made by using the circular orbit with radius $R = 3.0$.

transaxial cross sections of the phantom are depicted in Fig. 2, where the lower and upper bounds of the gray-level window were set to 0.99 and 1.05, respectively. To simulate tomographic measurements with a circular scan, we computed 240 cone-beam projections over 360° with 128 × 128 pixels in each projection. For the helical scan, we used $n \times 120$ projections acquired on a helix with $n = 6$ turns. The reconstructed image was represented by 128 × 128 × 128 voxels. The results for $R = 3.0$ are shown in Fig. 3. Note that we do not see deterioration of the density in the areas away from the plane of the circle, which is a characteristic artifact of the Feldkamp algorithm.[18] The reconstructed images are close to those of the phantom. The images obtained for the helix (Fig. 4) are similar to those for the circular orbit, and are very close to those of the phantom as well. To carry out a more quantitative comparison, we have depicted in Fig. 5 the intensity profiles along the line $(x, 0.25, -0.35)$

through the image. Here we can see that the single-circle orbit provides a certain bias in the reconstructed values, which is, however, relatively small. The helix also introduces small artifacts near the edges of the image. Nevertheless, both reconstructions are very close to the phantom and are similar to reconstructions obtained by more sophisticated algorithms.[18]

To study artifacts of the approximation more closely, we carried out a numerical experiment with a disk phantom. This phantom comprises seven equal ellipsoids with uniform density centered on the z axis. Figure 6
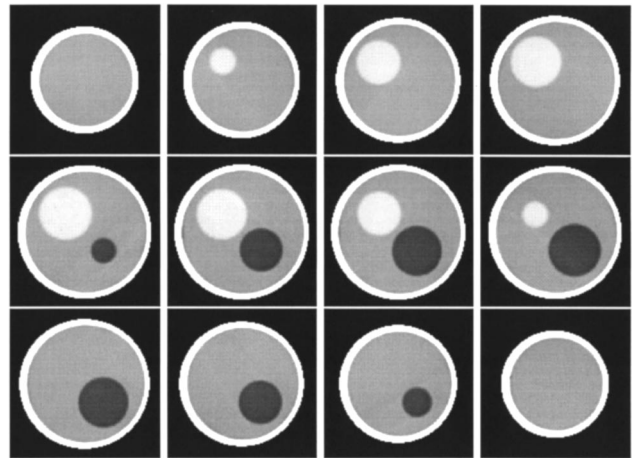
Fig. 4. Reconstructed images of the phantom. The reconstruction was made by using the helical orbit with radius $R = 3.0$ and number of turns $n = 6$.
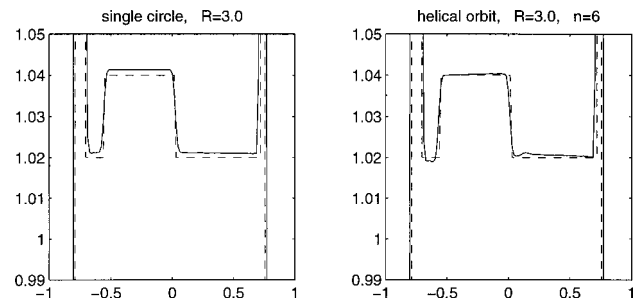
Fig. 5. Intensity profiles of the phantom and the reconstructed images along the line given by $(x, 0.25, -0.35)$. The profile of the phantom is shown by the dashed lines.
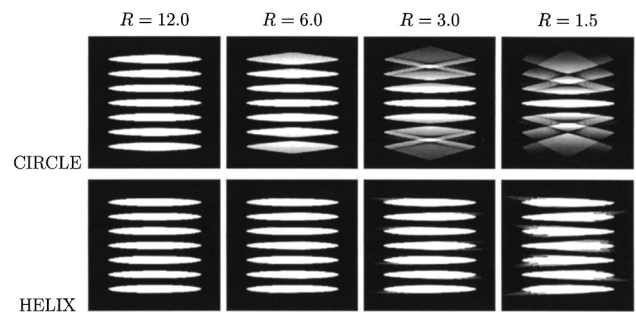
Fig. 6. Reconstructed images of the disk phantom; planes given by $y = 0$ are shown. The reconstructions were obtained by using the circular (upper row) and helical (lower row) orbits with variable radii $R = 12.0, 6.0, 3.0, 1.5$.

represents planes $y = 0$ of the images of the phantom reconstructed with the circular and helical orbits with four different radii: 12.0, 6.0, 3.0, and 1.5, where the whole range of image values is displayed. For the circular-scan reconstruction we used 120 projections, and helical reconstructions were obtained from $n \times 120$ projections with $n = 6$ turns of the helix. The circular-scan reconstruction made for $R = 12.0$ coincides well with the phantom and is practically the same as the helical-scan reconstruction. For $R = 6.0$, certain artifacts appear at the top and bottom of the image reconstructed with the circular orbit, whereas the helical reconstruction still has accurate shape and density. In the case of $R = 3.0$, the reconstruction with the single-circle orbit has large artifacts in the areas away from the central plane, which corresponds well with the results obtained by the Feldkamp algorithm.[18] The helical orbit provides more accurate reconstruction, although certain artifacts appeared along the edges of the disks. For $R = 1.5$, both reconstructions contain severe degradations of the shape and the density. However, in the case of the circular orbit, the central slice $z = 0$ is still reconstructed well, since the algorithm is reduced here to an exact fan-beam reconstruction formula. For the helical orbit, we observe typical artifacts of distortion of the shape of the disks, which can be reduced by minimizing the pitch of the helix.

7. CONCLUSION

By introducing a representation of the cone-beam transform through an integral equation whose kernel is the line delta function in 3D space, we have shown that the cone-beam reconstruction problem can be reduced to an image-restoration problem characterized by a shift-variant PSF. An analytical description of the PSF is given. To derive a shift-invariant approximation in the form of a convolution equation, we assume that the source is relatively far from the object to be reconstructed. The shift-variant PSF can then be reduced to a convolution kernel. Unlike the original Feldkamp algorithm[8] and the method by Peyrin *et al.*[32] our approach allows us to apply any source orbit that lies on a cylinder wrapping the object. The use of a specially chosen weighting factor in backprojection enables us to simplify the expression of the PSF and the reconstruction filter. A formula for such a shift-invariant filter of backprojections is given in the Fourier domain in the form of a 2D transaxial ramp filter. For the plane of the circular orbit, our algorithm coincides with an exact fan-beam reconstruction formula presented earlier.[29] One of the advantages of the algorithm is that it can be applied to the axially truncated data without any modification. Only 2D filtering in the transaxial planes is required, thereby shortening processing time. Nevertheless, it is a well-known fact that for accurate computation of deconvolution of the backprojection, the backprojection area has to be at least four times larger than the support of the image.[33] Thus it is very likely that the backprojection-and-filtering algorithm suggested is a few times slower than the Feldkamp algorithm; however, the optimization of the computer code and the detailed time comparison are possible subjects for further study. A numerical evaluation of the method has been made for the circular and helical orbits, where satisfactory results were obtained for both geometries. For instance, the results for the phantom simulating small differences in the density of tissue are very close to those that were previously obtained by reconstruction of the same phantom by the use of more sophisticated exact methods. For the circular orbit with radius $R = 3.0$, we do not see the characteristic density artifacts in the areas away from the central plane, which seem to be inherent for the Feldkamp algorithm. Such a good performance of our algorithm in this case can probably be explained by the fact that the density of the phantom varies insignificantly in the area that represents the tissue. This causes localization of the corresponding Fourier components about the origin, providing satisfactory approximation of the Fourier transform of the PSF by Eq. (22) even for relatively small radii of the orbit. Serious problems are more likely with objects whose density changes considerably along the z axis, causing the presence of large high-frequency components along the k_z axis in the Fourier domain. This is illustrated in the experiment with the disk phantom. For the circular orbit, we indeed observe strong density artifacts, which are very similar to those of the Feldkamp algorithm. At the same time, the use of the helical orbit helped us to improve the reconstruction for relatively small radii of the orbit, such as $R = 3.0$, that can be implemented in medical imaging.

The author can be reached at the address on the title page or by phone, 31-26-356-2791; fax, 31-26-351-5456; or e-mail, andrei@kema.nl.

REFERENCES

1. R. J. Jaszczak, K. L. Greer, and R. E. Coleman, "SPECT using a specially designed cone beam collimator," J. Nucl. Med. **29**, 1398–1405 (1988).
2. G. Gullberg, G. Zeng, F. L. Datz, P. E. Christian, C. H. Tung, and H. T. Morgan, "Review of convergent beam tomography in single photon emission computed tomography," Phys. Med. Biol. **37**, 507–534 (1992).
3. R. Clack and M. Defrise, "Cone-beam reconstruction by the use of Radon transform intermediate functions," J. Opt. Soc. Am. A **11**, 580–585 (1993).
4. C. Hamaker, K. T. Smith, D. C. Solmon, and S. L. Wagner, "The divergent beam X-ray transform," Rocky Mt. J. Math. **10**, 253–283 (1980).
5. F. Natterer, "Recent developments in X-ray tomography," Lect. Appl. Math. **30**, 177–198 (1994).
6. A. G. Ramm and A. I. Katsevich, *The Radon Transform and Local Tomography* (CRC Press, Boca Raton, Fla., 1996).
7. P. Grangeat, "Mathematical framework of cone-beam 3D reconstruction via the first derivative of the Radon transform," Vol. 1497 of Lecture Notes in Mathematics, G. T. Herman, A. K. Louis, and F. Natterer, eds. (Springer-Verlag, Berlin, 1991), pp. 66–97.
8. L. A. Feldkamp, L. C. Davis, and J. W. Kress, "Practical cone-beam algorithm," J. Opt. Soc. Am. A **1**, 612–619 (1984).
9. B. D. Smith, "Cone-beam tomography: recent advances and tutorial review," Opt. Eng. **29**, 524–534 (1991).
10. A. V. Bronnikov and G. Duifhuis, "Wavelet-based image enhancement in x-ray imaging and tomography," Appl. Opt. **37**, 4437–4448 (1998).
11. A. A. Kirillov, "On a problem of I. M. Gel'fand," Sov. Math. Dokl. **2**, 268–269 (1961).
12. H. K. Tuy, "An inversion formula for cone-beam reconstruction," SIAM J. Appl. Math. **43**, 546–552 (1983).

13. B. D. Smith, "Image reconstruction from cone-beam projections: necessary and sufficient conditions and reconstruction methods," IEEE Trans. Med. Imaging **4**, 14–25 (1985).

14. H. H. Barrett and H. Gifford, "Cone-beam tomography with discrete data sets," Phys. Med. Biol. **39**, 451–476 (1994).

15. S. Webb, J. Sutcliffe, L. Burkinshow, and A. Horsman, "Tomographic reconstruction from experimentally obtained cone-beam projections," IEEE Trans. Med. Imaging **6**, 67–73 (1987).

16. Z. J. Cao and B. M. W. Tsui, "A fully three-dimensional reconstruction algorithm with the nonstationary filter for improved single-orbit cone beam SPECT," IEEE Trans. Nucl. Sci. **40**, 280–287 (1993).

17. H. Kudo and T. Saito, "Feasible cone beam scanning methods for exact reconstruction in three-dimensional tomography," J. Opt. Soc. Am. A **7**, 2169–2183 (1990).

18. H. Kudo and T. Saito, "Derivation and implementation of a cone-beam reconstruction algorithm for nonplanar orbits," IEEE Trans. Med. Imaging **13**, 196–211 (1994).

19. G. Zeng and G. Gullberg, "A cone-beam tomography algorithm for orthogonal circle-and-line orbit," Phys. Med. Biol. **37**, 563–577 (1992).

20. X. Yan and R. M. Leahy, "Cone beam tomography with circular, elliptical and spiral orbits," Phys. Med. Biol. **37**, 493–506 (1992).

21. G. Wang, T.-H. Lin, P. Cheng, and D. M. Shinozaki, "A general cone-beam reconstruction formula," IEEE Trans. Med. Imaging **12**, 486–496 (1993).

22. M. Defrise and R. Clack, "A cone-beam reconstruction algorithm using shift-variant filtering and cone-beam backprojection," IEEE Trans. Med. Imaging **13**, 186–195 (1994).

23. C. Axelsson and P. E. Danielsson, "Three-dimensional reconstruction from cone-beam data in $O(N^3 \log N)$ time," Phys. Med. Biol. **39**, 477–491 (1994).

24. S. Schaller, T. Flohr, and P. Steffen, "An efficient Fourier method for 3-D Radon inversion in exact cone-beam CT reconstruction," IEEE Trans. Med. Imaging **17**, 244–250 (1998).

25. M. Seger, "Three-dimensional reconstruction from cone-beam data using an efficient Fourier technique combined with a special interpolation filter," Phys. Med. Biol. **43**, 951–959 (1998).

26. H. Kudo and T. Saito, "Fast and stable cone-beam filtered backprojection method for non-planar orbits," Phys. Med. Biol. **43**, 747–760 (1998).

27. F. Noo, M. Defrise, and R. Clackdoyle, "Single-slice rebinning method for helical cone-beam CT," Phys. Med. Biol. **44**, 561–570 (1999).

28. M. Defrise, R. Clack, and D. Townsend, "Solution to the three-dimensional image reconstruction problem from two-dimensional parallel projections," J. Opt. Soc. Am. A **10**, 869–877 (1993).

29. G. Gullberg, "The reconstruction of fan-beam data by filtering the back-projection," Comput. Graph. Image Process. **10**, 30–47 (1979).

30. F. Peyrin, "The generalized back-projection theorem for cone beam projection data," IEEE Trans. Nucl. Sci. **32**, 1512–1519 (1985).

31. Z. H. Cho, E. X. Wu, and S. K. Hilal, "Weighted backprojection approach to cone beam 3D projection reconstruction for truncated spherical detection geometry," IEEE Trans. Med. Imaging **13**, 111–121 (1994).

32. F. Peyrin, R. Goutte, and M. Amiel, "Analysis of a cone beam x-ray tomographic system for different scanning modes," J. Opt. Soc. Am. A **9**, 1554–1563 (1992).

33. S. W. Rowland, "Computer implementation of image reconstruction formulas," in *Image Reconstruction from Projections*, G. T. Herman, ed. (Springer-Verlag, Berlin, 1979), pp. 9–79.